

A mouse model of volumetric muscle loss and therapeutic scaffold implantation

Caroline Hu¹, Gladys Chiang¹, Alex H.-P. Chan © ^{2,3}, Cynthia Alcazar⁴, Karina H. Nakayama⁴, Marco Quarta¹, Thomas A. Rando © ^{1,5} & Ngan F. Huang © ^{1,2,3,6} ⊠

Abstract

Skeletal myofibers naturally regenerate after damage; however, impaired muscle function can result in cases when a prominent portion of skeletal muscle mass is lost, for example, following traumatic muscle injury. Volumetric muscle loss can be modeled in mice using a surgical model of muscle ablation to study the pathology of volumetric muscle loss and to test experimental treatments, such as the implantation of acellular scaffolds, which promote de novo myogenesis and angiogenesis. Here we provide step-by-step instructions to perform full-thickness surgical ablation, using biopsy punches, and to remove a large volume of the tibialis anterior muscle of the lower limb in mice. This procedure results in a reduction in muscle mass and limited regeneration capacity; the approach is easy to reproduce and can also be applied to larger animal models. For therapeutic applications, we further explain how to implant bioscaffolds into the ablated muscle site. With adequate training and practice, the surgical procedure can be performed within 30 min.

Key points

- A surgical procedure for the full-thickness surgical ablation of ~20–60% of the mouse tibialis anterior using a commercial 2–3-mm biopsy punch allows the ablation size to be customized. The model is representative of skeletal muscle loss.
- The surgically ablated muscles' uniform geometry does not fully reproduce the complexity of traumatic muscle injury, which includes other injuries associated with trauma to the bone, nerves or tendons.

Key references

Hu, C. et al. *Bioengineering* **9**, 37 (2022): https://doi.org/10.3390/bioengineering9010037

Alcazar, C. A. et al. *Biomat*. *Sci.* **8**, 5376–5389 (2020): https://doi.org/10.1039/d0bm00990c

Quarta, M. et al. *NPJ Regen. Med.* **3**, 18 (2018): https://doi.org/10.1038/s41536-018-0057-0

Quarta, M. et al. *Nat. Commun.* **8**, 15613 (2017): https://doi.org/10.1038/ncomms15613

¹Veterans Affairs Palo Alto Health Care System, Palo Alto, CA, USA. ²The Stanford Cardiovascular Institute, Stanford University, Palo Alto, CA, USA. ³Department of Cardiothoracic Surgery, Stanford University, Palo Alto, CA, USA. ⁴Department of Biomedical Engineering, Oregon Health and Science University, Portland, OR, USA. ⁵Department of Neurology, University of California Los Angeles, Los Angeles, CA, USA. ⁶Department of Chemical Engineering, Stanford University, Palo Alto, CA, USA. E-mail: ngantina@stanford.edu

Introduction

Volumetric muscle loss (VML) is characterized by the loss of a large portion of skeletal muscle, resulting in impaired function¹. In humans, it can result from traumatic injuries or vehicle accidents that lead to extensive muscle and bone damage. Skeletal muscle is normally highly regenerative, owing to the presence of satellite cells that give rise to newly formed muscle fibers². However, depending on the severity of the muscle injury, the satellite cell population may not be able to compensate for large tissue loss, resulting in fibrosis rather than muscle formation³-⁵. The pathophysiological features of VML injuries include irreversible muscle impairment, muscle mass loss and intramuscular fibrosis characterized by collagen deposition⁶.

Standard treatment approaches for VML currently include physical therapy and autologous muscle grafts, which have shown limited effects on myofiber regeneration or restoration of function $^{7.8}$. Muscle flap transfer requires surgical dexterity and is complicated by limited donor tissue reserves and donor site morbidity 1,9,10 . Owing to the drawbacks of surgical intervention, more recent strategies aim to deliver therapeutic cells and structural scaffolds to promote revascularization and myofiber regeneration in the affected areas $^{1.11}$.

Development of the protocol

The development of cell and/or biomaterials therapies for the treatment of VML requires the use of a robust animal model that replicates the severity of tissue damage, as well as pathology, of muscle injury found in humans. Experimentally induced models of VML are based on the surgical ablation of specific muscle groups. This surgical model is based on a prior biopsy punch ablation model established in rodents that entails applying a biopsy punch to the tibialis anterior (TA) muscle to create a defined cylindrically shaped muscle defect^{12–14}. Here we describe the procedure for a reproducibly inducing VML in mice, which we have previously successfully utilized¹⁵. We adapt the biopsy punch procedures for the induction of VML in mice^{16–18} and further include the steps for the implantation of biological scaffolds into the ablated muscle region.

Overview of the protocol

The mouse model of VML is obtained via the full-thickness surgical ablation of ~20% or ~60% of the TA muscle mass. The major steps are an incision to the skin, biopsy punch ablation and then surgical implantation of a biomaterial at the site of ablation. The muscle ablation is performed using a commercial 2-mm or 3-mm biopsy punch. The different biopsy punch sizes allow the ablation size to be customized. Although the relationship between ablation size and severity of injury is understudied 12 , the muscle ablation size is an important design criterion. To demonstrate the feasibility of this approach, we explain how to induce the VML model using C57BL/6J mice (18 weeks old, male), in which two adjoining 2-mm punch full-thickness ablations reflect ~20% muscle mass ablation, whereas two adjoining 3-mm full-thickness punch ablations reflect ~60% ablation (Table 1 and Fig. 1). To assess the subsequent changes in muscle structure and function, we chose timepoints of 3–4 weeks after surgery, as this is a timeframe that permits the assessment of muscle structure and function, although longer time points can also be used to study the long-term effects of VML.

 ${\bf Table 1} | {\bf Characterization\ of\ full-thickness\ ablation\ dimensions\ in\ the\ TA\ muscle\ using\ two\ 2-mm\ or\ 3-mm\ biopsy\ punches$

Parameter	2-mm punch	3-mm punch
Percentage of TA weight removed on day 0 (mean ± s.d.)	17.5 ± 8.9%°	58.4 ± 11.1%
TA weight removed (day 0) (mean ± s.d.)	8.5 ± 4.4 mg	28.5 ± 5.4 mg
TA weight (day 21) (mean ± s.d.)	54.2 ± 7.2 mg ^b	34.9 ± 6.8 mg

Data are derived from 18-week-old C57/BL6 mice. $^{\circ}$ Statistically significantly different from 3-mm punch (n = 5, 2-mm punch group; n = 6, 3-mm punch group), Student's t-test ($P \le 0.0001$). $^{\circ}$ Statistically significantly different from 3-mm punch, Student's t-test ($P \le 0.0005$). Source Data.

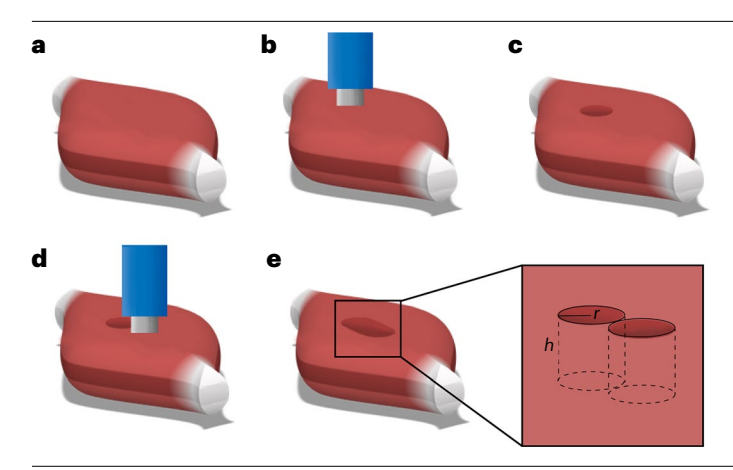


Fig. 1| **Schematic overview of creating VML injury to the TA muscle using a biopsy punch. a**, Diagram of the TA muscle. **b**, An initial punch is made to create a full-thickness muscle defect. A spatula is placed behind the TA. **c**, The resulting ablation is 2 mm in diameter and 4 mm deep. **d**, A second biopsy punch is created adjacent to the first to expand the size of the ablation. **e**, The ablated muscle volume derived from two punches is estimated by $2\pi r^2 h$, where muscle thickness is represented by h = 4 mm and r is the punch radius, as indicated by the inset.

Advantages and limitations

Compared with other procedures that involve surgically ablating a muscle defect with other defined shapes 19 , this biopsy punch model is well suited for users with limited surgical training. The rodent models of VML can further be combined with voluntary exercise and/or engineered tissue-based therapies 11,19,20 .

A limitation of surgical ablation-mediated VML is that the uniform geometry of the ablated muscle does not fully mimic the complex geometries that result from traumatic muscle injury. This model is representative of skeletal muscle loss but does not reproduce other injuries associated with trauma to the bone, nerves or tendons.

A limitation associated with scaffold implantation is that suturing of the TA muscle after scaffold placement can alter the force or torque produced, since the structure of the muscle fibers will have changed. Additionally, only scaffolds with sufficient structural integrity can be sutured to the adjacent muscle, whereas soft biomaterials or hydrogels should be injected or otherwise placed into the ablation region. Despite the limitations and design considerations, this VML procedure is reproducible and requires minimal surgical expertise, which is well suited for beginners of VML preclinical research.

Applications

After generating the VML model, we further cover the implantation of acellular scaffolds into the ablated muscle as an experimental therapy. Such scaffolds can be generated from naturally derived extracellular matrix proteins or synthetic polymers. More generally, there is a wide range of experimental therapies that can be tested in muscle injury models, including cell-seeded scaffolds 11,19,21,22, decellularized extracellular matrix scaffolds 33 and drug/gene-releasing scaffolds 15,24,25. Alternatively, minced muscle grafts 6 or therapeutic cells 927 can be transplanted for muscle repair. These experimental treatments can be delivered acutely after the VML induction or at later timepoints when chronic VML has already been established. Furthermore, these experimental therapies can also be tested concurrently with rehabilitative strategies such as physical exercise 15,20.

Alternative methods

For the procedure detailed here, we selected the induction of VML in the mouse TA muscle, owing to its relatively simple geometry and its parallel fusiform muscle structure 19,28,29 . Furthermore, the TA model is clinically relevant, owing to the high number of clinical cases of extremity wounds caused during military conflicts 30 . Alternative animal models of VML include muscle ablation to the gastrocnemius 31 , the rectus abdominis 32 , the latissimus dorsi 22 and the quadriceps muscles 12 .

Experimental design

Previous studies have shown that a 20-30% muscle ablation is sufficient to impair muscle force generation and vascular function ^{15,18,28,33,34}. However, larger degrees of muscle ablations can simulate varying degrees of muscle trauma. In the protocol, we cover a range of muscle

injuries, from ~20–60% muscle ablation. Following two overlapping biopsy punch ablations, the ablated muscle takes the shape of an oblong-shaped defect at the center of the TA muscle (Fig. 1). Increasing the number of biopsy punch ablations can further increase the muscle ablation size to represent a more severe clinically relevant muscle loss. We use a full-thickness model, in which the muscle is ablated through its entire depth. This model is more severe than the partial thickness ablation model, in which the ablation affects only a portion of the muscle depth, leaving some proportion of muscle remaining completely intact.

This procedure is suitable for both unilateral and bilateral surgical ablation to the TA muscle of the hind legs. The bilateral surgical model permits simultaneous analysis of two treatment groups within the same animal. However, it has been reported that isometric torque values were higher in bilateral VML models than in unilateral VML models³⁵. Therefore, differences in potential muscle loading should be considered when deciding between bilateral and unilateral models.

This surgical procedure can be adapted for mice of varying strains, sexes and ages. We typically induce VML in C57BL/6J mice owing to the predominance of this strain in preclinical research. However, VML can be induced in most mouse strains. For nonallogenic cell delivery, we use nonobese diabetic/severe combined immunodeficiency (NOD/SCID) mice to obviate concerns of immune rejection. Mice as young as 7–8 weeks can be used depending on the study design. However, since muscle mass and dimensions vary with age, it is necessary to adjust the dimensions to accurately reproduce a consistent volume of muscle ablation. For example, the ablation dimensions for 18-week-old C57BL/6 mice are presented in Table 1.

Although larger animal models (such as sheep or pigs) are closer in size to a human 18,36-38, mice are a good option for the initial preclinical testing of therapeutic strategies in VML because of their ease of handling, reduced cost and availability in research facilities, and rodents further allow the use of transgenic strains to study the molecular underpinnings of VML. Force or torque measurements can be used to assess muscle function 21, and histological analyses can provide insight into the cellular composition and morphology of the injured muscle 19,20,28.

Regardless of the experimental design, it is also necessary to include appropriate controls for the experiments, such as a no-surgery age-matched control, a sham surgery control and a VML lesion with no treatment control group for comparison. Where appropriate, the inclusion of a reference control scaffold should be considered. Typical cohort sizes range from 5 to 12 animals per group to account for intragroup variances.

Regulatory approvals

All animal procedures must be reviewed and approved by the institutional animal care and use committee, as was done for the studies in this work, or other relevant institutional guidelines.

Materials

Animals

Experimental mice greater than 7 weeks old (the Jackson Laboratory)
 CAUTION The use of experimental mice must be in compliance with national and institutional regulations related to the use of animals for research purposes. Permissions to carry out experiments should be obtained before the start of animal studies.

Reagents

- 10% Povidone-iodine solution swabsticks (Fisher Scientific, cat. no. 19-065534 or equivalent)
- 70% Isopropyl alcohol swabsticks (Fisher Scientific, cat. no. 13-680-63 or equivalent)
- Isoflurane (RWD Life Science, cat. no. R510-22-10 or equivalent)
- Veet depilatory cream (Amazon, cat. no. BOODTCOCL8 or equivalent)
- Ophthalmic ointment (Puralube Ophthalmic Ointment, Patterson Veterinary, cat. no. 07-888-2572 or equivalent)

- Buprenorphine extended release 0.5 mg/mL (Wedgewood Pharmacy, cat. no. BUPREN-INJ010VC or equivalent)
- Enrofloxacin antibacterial injectable solution 2.27% (Covetrus, cat. no. 074743 or equivalent)
- Optimal cutting temperature (OCT) compound (Fisher Scientific, cat. no. 23-730-571)

Equipment

- Electric hair clippers (Amazon, cat. no. B00068EXQ8 or equivalent)
- Surgical microscope (Zeiss, Opmi 6-SDFC, cat. no. OPMI6SDFC or equivalent)
- Heat therapy pump with warming pad (Adriot Medical Systems, cat. no. HTP-1500 or equivalent)
- RC2 rodent circuit controller anesthesia system (VetEquip, cat. no. 922100 or equivalent)
- Microbead sterilizer (Fisher Scientific, cat. no.14-955-341 or equivalent)
- Ear tags (Fisher Scientific, cat. no. NC9208405 or equivalent)
- Ear tag applicator (Fisher Scientific, cat. no.NC0038715 or equivalent)
- Sterile drape (Fisher Scientific, cat. no. 19-310-671 or equivalent)
- Sterile gauze (Fisher Scientific, cat. no. 22-362178 or equivalent)
- Size 11 scalpel (Fisher Scientific, cat. no.14-840-01 or equivalent)
- Calipers (Fine Science Tools, cat. no. 30087-20 or equivalent)
- 8-0 Nylon sutures (Fine Science Tools, cat. no. 12051-08)
- Fine scissors (Fine Science tools, cat. no. 14060-09 or equivalent)
- Sterile biopsy punch, 2 mm (Med Vet International, cat. no. BP2MMX25 or equivalent)
- Sterile biopsy punch, 3 mm (Med Vet International, cat. no. BP3MMX25 or equivalent)
- Chemi-Scraper spatula (Fisher Scientific, cat. no. 14-373 or equivalent)
- Dumont no. 7 forceps (Fine Science Tools, cat. no. 11272-40)
- Dumont no. 5/45 forceps (Fine Science Tools, cat. no. 11251-35)
- Castroviejo micro needle holders (Fine Science Tools, cat. no. 12060-01)
- Cryomolds, 15 mm × 15 mm × 5 mm (Fisher Scientific, cat. no. NC9642669 or equivalent)
- 3M Transpore surgical tape (Fisher Scientific, cat. no. 18-999-381 or equivalent)
- Sharpie permanent marker (Sanford, cat no. SAN38264PP or equivalent)

Procedure

▲ CRITICAL Procedures must be reviewed and approved by the institutional animal care and use committee or other relevant institutional guidelines.

Preoperative steps (day of surgery, before first incision)

● TIMING 20 min

- 1. Anesthetize the mouse by placing it in an isoflurane induction chamber. Induce the animal with 3–5% isoflurane and 100% oxygen at a flow rate of 1 L/min.
- 2. Remove the animal from the induction chamber and place the animal on a preoperative site with an isoflurane nose cone.
- Reduce the isoflurane to a maintenance level of 1–2% isoflurane and 100% oxygen at a flow rate of 1 L/min.
- 4. Position the animal in a supine position.
- 5. Use clippers to remove the hair from the hind limb from as proximal as the thigh to as distal as the ankle.
- 6. To remove excess small hairs, apply depilation cream (Veet) and a cotton swab to massage the cream onto the skin. Let the cream sit for 30 s to 1 min. Remove the cream with gauze. Remove excess cream with alcohol swabs or water.
- 7. Identify each animal in a cohort using one of two methods:
 - (A) Method 1: tag the animal with a unique metal ear tag or ear punch.

- (B) Method 2: mark the tail with a unique marking scheme. Each cage is assigned a unique color using a Sharpie marker. Mice within the same cage are marked with the same color but differentiated by the number of lines for identification. The tails should be remarked twice a week or when the marker ink begins to fade away.
- 8. Create a sterile operative site by taping down a sterile drape over a warming plate that is set to 37 °C.
- 9. Make a pillow out of sterile gauze to prop up the hind leg for surgery and tape it down to the operative site. Place the animal in a supine position and rest the hind limb on the gauze pillow with surgical tape.
- 10. Align the femur in a neutral position, parallel to the long axis of the body, making sure that the ankle joint is plantarflexed so that the toes are pointed inferiorly and secured with surgical tape.
- 11. Reduce the isoflurane to a maintenance level of 1.5-2% isoflurane and 100% oxygen at a flow rate of $1L/\min$. The maintenance level may vary between animals.
- 12. Administer preoperative buprenorphine extended release analgesia (0.6–1.0 mg/kg and antibiotics (enroflaxacin, 5 mg/kg) before the first incision according to institutional guidelines.
- 13. Aseptically prepare the leg by alternating betadine and alcohol, three times.
- 14. Begin the sterilization at the center of the limb and spiral outward in a clockwise direction.
- 15. After the last alcohol clean, allow the limb to dry for 30 s.
- 16. Place a sterile drape over the limb.
- 17. Check the depth of anesthesia by performing a toe-pinch test. Proceed with the surgery if there is no reflex response.

Operative procedure

● TIMING 20 min per lea

▲ CRITICAL Conduct all operative procedures following aseptic techniques.

18. With a size 11 blade scalpel, make a longitudinal incision in the skin from as proximal to the knee joint to as distal to the ankle joint (Fig. 2a).

◆ TROUBLESHOOTING

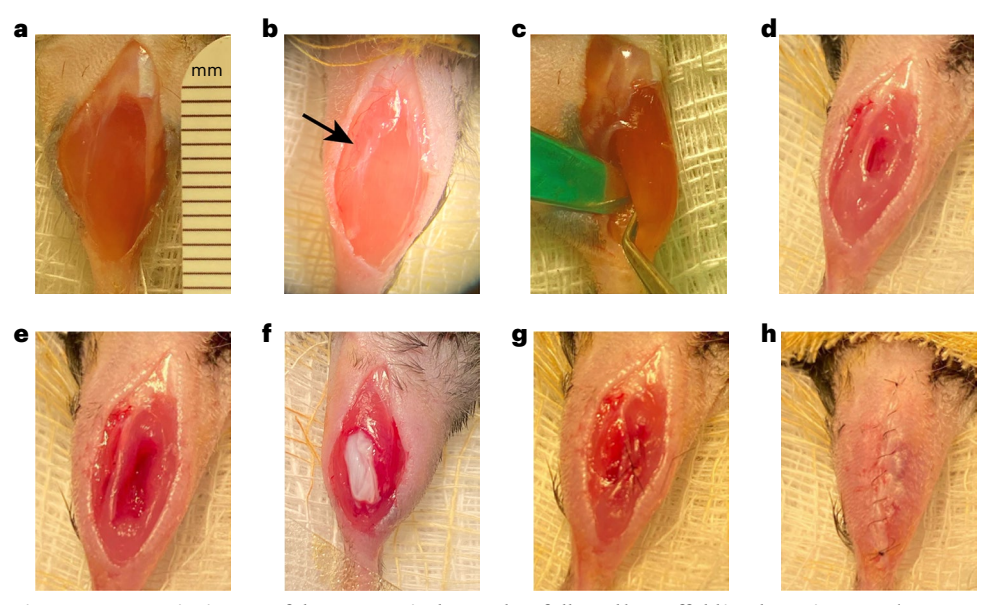


Fig. 2| **Intraoperative images of the VML surgical procedure followed by scaffold implantation. a**, A skin incision exposes the TA muscle. The ruler in the photo depicts increments in mm. **b**, The fascia is cut to expose the TA. The arrow indicates the fascia. **c**, A metal spatula is placed directly beneath the TA muscle. **d**, The morphology of the TA muscle is shown after the initial punch ablation, measuring 2 mm in diameter and 4 mm in depth. **e**, The morphology of the TA is shown after a second biopsy punch ablation adjacent to the first. **f**, A collagen scaffold is implanted into the region of ablation. **g**, The muscle is closed with sutures. **h**, The skin after closure with suture.

- 19. Using forceps, gently lift the thin fascia up away from the TA muscle and use scissors to cut it parallel to the length of the muscle to expose the width of the TA (Fig. 2b).
- 20. Surgically dissect the TA from the extensor digitorum longus (EDL) muscle using the scalpel and place the spatula between the TA and the EDL (Fig. 2c).
- 21. Using the biopsy punch, create a defect just above the midline of the TA, pushing the biopsy punch until it contacts the spatula to ensure a full-thickness model.

 ▲ CRITICAL STEP When pressure from the biopsy punch is applied, the muscle tissue below it may move, leading to the ablated tissue being smaller than the size of the punch. Securing the periphery of the muscle group with hands or other appropriate tools in a sterile manner will help it retain its original shape so that the expected volume of tissue is removed. (Fig. 2d).

◆ TROUBLESHOOTING

- 22. Make an overlapping punch adjacent to the first ablation, using the same technique as previously stated, to create a defect with oblong shape (Fig. 1d,e and Fig. 2e).

 ▲ CRITICAL STEP If applicable to the study, weigh the tissue that was removed after this step. The size of the ablation resulting from adjoining 2-mm or 3-mm diameter punches (Fig. 2e) is presented in Table 1 for 18-week-old mice. Optional: depending on the age and weight of the mice, the percentage ablation volume created by the punches may vary and should be determined in initial studies.
- 23. Scaffolds should be shaped to fit into the size of the ablation, leaving room for the muscle incision site to be closed (Fig. 2f).
 - (A) Optionally, scaffolds with sufficient structural integrity can be further sutured to adjacent muscle for increased stability.
 - (i) Suture the muscle with 8-0 vicryl sutures in an X fashion to secure the scaffold inside the ablated muscle³⁹ (Fig. 2g).
 - (ii) Use two double knots to close the muscle. Note that suturing might alter the muscle architecture and force transmission along the muscle fibers.
- 24. Suture the skin with 8-0 vicryl suture by anchoring on the proximal end of the incision and using a continuous stitch pattern toward the distal end (Fig. 2h).

◆ TROUBLESHOOTING

- 25. Apply antibiotic ointment to the incision site.
- 26. For bilateral studies, repeat the day-of-surgery preoperative steps and operative procedure for the other TA muscle, as desired.
- 27. Place the animal in a recovery cage with a warming base. Monitor the animal's respiratory rate for 15 min or until fully conscious. Return the animal to group housing.
- 28. Monitor the animal for signs of pain or distress in compliance with institutional animal care and use policies. Use the Mouse Grimace Scale to identify signs of pain ⁴⁰. If signs of pain persist 72 h after the first injection of buprenorphine extended release, administer another dose and contact a veterinarian for a consultation.
- 29. Imaging and muscle physiology measurements can be carried out at various time points, before euthanasia and tissue collection.

Euthanasia

● TIMING 10 min

- 30. At the end of the experiment, commonly at 3 weeks after the induction of muscle ablation, euthanize the animal with CO_2 or isoflurane overdose. Confirm euthanasia was successful by absence of diaphragm movement and heartbeat.
- 31. Perform an approved secondary form of euthanasia, such as cervical dislocation, by applying pressure to the neck to sever the spinal column from the skull.

Postmortem tissue collection

● TIMING 5 min

32. After euthanasia, explant both TA muscles from the hind limb. Use forceps and scissors to cut the skin laterally around the ankle. Insert the scissors underneath the skin and cut longitudinally up to the thigh.

- 33. Expose the leg muscle groups by peeling back the skin from the ankle to the thigh.
- 34. Anchor the foot down with tape if needed.
- 35. Locate the TA tendon on the distal end of the TA muscle. While gripping the tendon, insert the tip of the scalpel against the distal end of the tibia and glide the scalpel proximally along the tibia until it reaches the lateral patellar retinaculum to separate the connecting fascia of the TA muscle and the tibia periosteum (Supplementary Video 1).
- 36. Isolate the TA muscle. Using fine forceps, gently separate the fascia beneath the tendon by sliding the forceps along the dorsal side of the tendon and sever it using a scalpel. Use forceps to lift and separate the TA muscle from the adjacent soleus and EDL muscle (Supplementary Video 1).
 - ▲ CRITICAL STEP Be careful not to damage the TA muscle by accidentally removing part of the muscle during the collection step.
 - **◆ TROUBLESHOOTING**
- 37. For cryosectioning, place the TA muscle in a cryomold filled with OCT freezing media and then snap freeze the mold in a bath of 2-methylbutane on dry ice.
 - (A) (Optional): note that if muscle fiber length should be maintained, first pin the explanted muscle to cork and then freeze in 2-methylbutane bath on dry ice, followed by embedding into OCT.
 - **◆ TROUBLESHOOTING**
 - (B) Store the cryomold at -80 °C.
- 38. Alternatively, tissues can be processed for routine paraffin embedding.

Troubleshooting

Troubleshooting advice can be found in Table 2.

Table 2 | Troubleshooting

Step	Problem	Possible reason	Solution
18-24	TA muscle is dry	Not enough saline is being periodically placed on the muscle	Use a sterile swab dipped in saline to moisten the TA muscle more often
21	Biopsy punches are ablating uneven or less than expected amounts of tissue	The muscle is not especially stiff, so it can slide around when the pressure from the biopsy punch is applied to it	Use the spatula on the underside of the muscle to help stabilize it so that it does not unexpectedly move while ablating tissue. In addition, securing the periphery of the muscle group with hands or other appropriate tools in a sterile manner will help it retain its original shape so that the expected volume of tissue will be removed
24	Mice rip out sutures	Mice may find sutures uncomfortable	Use interrupted sutures instead of a continuous stitch so that the incision does not completely open
36	Part of the TA muscle is damaged when collecting the muscle	When collecting the TA, the scalpel may accidentally remove part of the muscle	Remove muscles of anterior compartment by cutting the distal tendons and cutting at the proximal end. Then separate the TA from the other muscles using forceps
38	Tissue for histology shows degradation and/or artifacts	Tissue that is embedded in OCT without fixing can lead to tissue degradation or artifacts	Fix tissue in formalin immediately after collection and embed in paraffin

Timing

Steps 1–17, preoperative steps (day of surgery, before first incision): 20 min

Steps 18–29, operative procedure: 20 min per leg

Steps 30-31, euthanasia: 10 min

Steps 32–38, postmortem tissue collection: 5 min

Anticipated results

Characterizing VML ablation by weight

In 18-week-old C57BL/6 mice that undergo a VML surgery using either a 2-mm or 3-mm diameter biopsy punch, the resulting ablation dimensions and size are shown in Table 1. A 2-mm punch removes ~17% of the muscle, whereas the 3-mm punch removes ~58% of the TA muscle. When the 2-mm punch is used in 8-week-old C57BL/6 mice, the mass of ablated muscle is ~20% of the muscle instead of 17%, probably due to the difference in size and muscle gain experienced by mice as they age 15 . The 18-week-old C57BL/6 mouse TA muscles were collected 21 d after surgery and weighed. The weight of the TA muscle in the 3-mm punch group was significantly smaller than the 2-mm punch group, based on statistical analysis by a Student's t-test. This indicates that the 3-mm group retains greater muscle loss than the 2-mm group after 3 weeks, as is expected from a more severe degree of muscle ablation.

Torque production of TA muscle post-injury

To assess the functional deficit of the VML model, muscle force or torque testing can be performed using muscle physiology equipment from companies such as the Aurora Scientific 3-in-1 Whole Animal System. Mice are anesthetized and their hindlimbs are shaved before placement onto the frame. The knee joints are stabilized, and the foot is attached to a footplate. Needle electrodes are then inserted percutaneously to stimulate the anterior crural compartment. Compared with the uninjured healthy control mice, the mice with 2-mm and 3-mm punch ablations show significant torque reduction at 21 d postablation (Fig. 3a). Functional deficit is relatively more pronounced in mice that receive muscle ablation from the 3-mm punch, as showed by the significantly reduced torque production, in comparison with the 2-mm group, based on analysis of variance with Tukey post hoc testing (Fig. 3a).

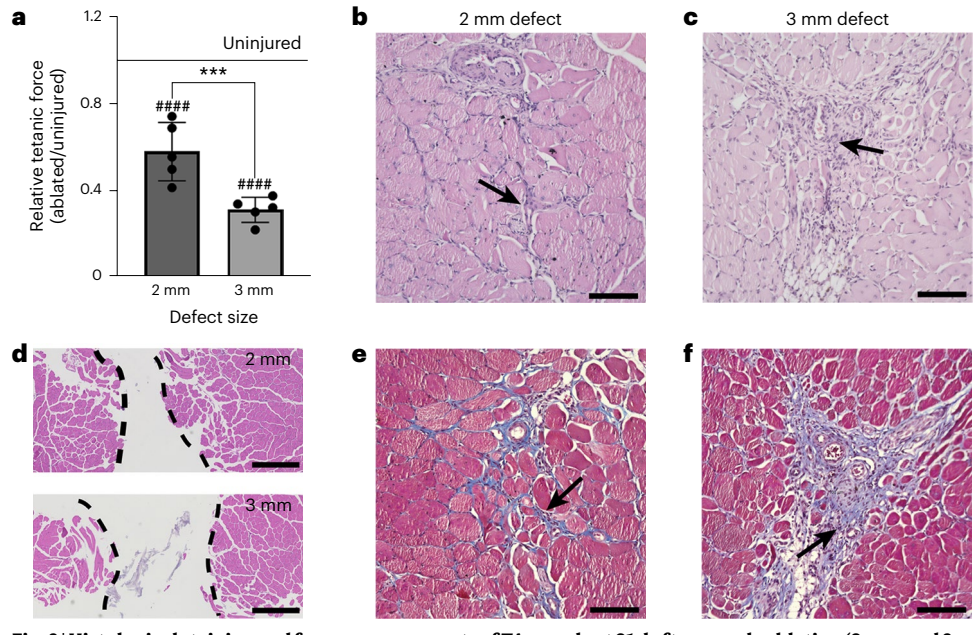


Fig. 3 | Histological staining and force measurements of TA muscle at 21 d after muscle ablation (2-mm and 3-mm models). a, Torque measurements from tetanic contraction of the anterior crural muscles that include the TA muscle, based on analysis of variance with Tukey's post hoc test. Data are shown relative to that of the uninjured muscle (n=5, ****P<0.0001 for the indicated pair-wise comparison; ****P<0.0001 when compared with the uninjured group). b,c, H&E staining of TA muscles after ablation using the 2-mm (b) or 3-mm (c) biopsy punch. d, Cross-sectional region of the TA immediately postsurgery shows the muscle gap after biopsy punch, as denoted by the dotted lines. e,f, Images show Masson's trichrome staining of TA muscle using a 2-mm (e) or 3 mm (f) biopsy punch. Arrows indicate the areas of fibrotic connective tissue and disorganized myofibers. Scale bar, 500 μ m for d and 100 μ m for b,c,e and f.

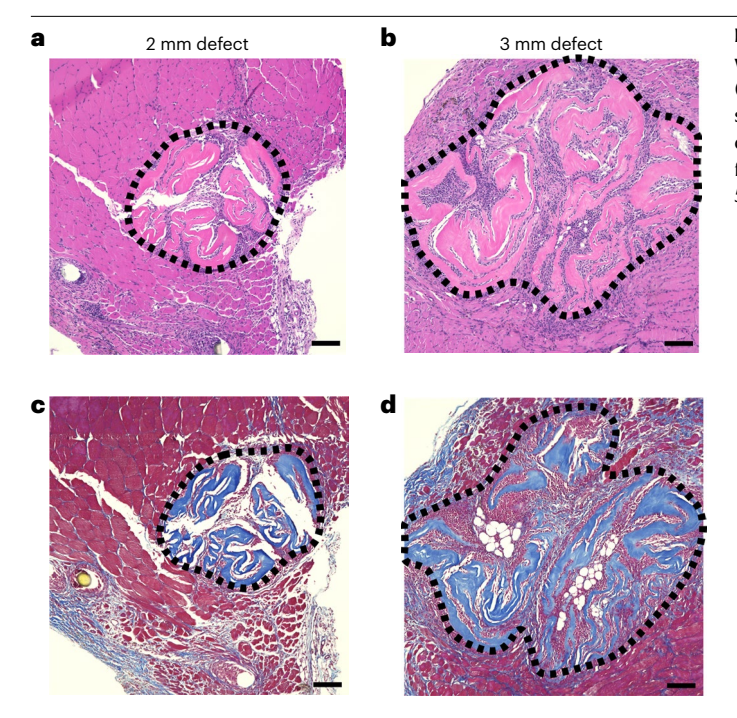


Fig. 4 | Histological staining of TA muscle at 3 weeks after muscle ablation with collagen scaffold implantation. a,b, H&E stain of TA ablation using a 2-mm (a) or 3-mm (b) biopsy punch, followed by implantation of a nanofibrillar collagen scaffold into the defect. c,d, Masson's trichrome stain visualizes the nanofibrillar collagen scaffold in blue after implantation into the 2-mm (c) or 3-mm (d) defect for 3 weeks. The dotted line denotes the region of scaffold implantation. Scale bar, 500 μ m.

Previous studies by other groups employing surgical ablation of the TA muscle in rodents also show limited muscle regeneration. In a rat VML model involving 20% TA ablation, the muscle was unable to substantially regenerate after 4 weeks, and muscle physiology shows a notable reduction in torque that is consistent with persistent functional impairment⁴¹. In alignment with these results, we show in this mouse VML model that there is significantly reduced torque generation at 21 d postsurgery, compared with uninjured animals (Fig. 3a).

Histological assessment of TA muscle after VML

Tissue sections at 21 d postsurgery were stained using hematoxylin and eosin (H&E) and Masson's trichrome stains to visualize tissue morphology (Fig. 3b-f). With the closure of the muscle after ablation, the borders of the ablation site can become less evident. Trichrome staining of the tissue sections allows for visualization of collagen deposition. The 3-mm punch group shows higher levels of collagen and disorganized myotubes in the region of the ablation, compared with the 2-mm punch group (Fig. 3e,f). Excess collagen deposition is characteristic of VML, as well as increasing muscle stiffness^{13,36}.

When the ablated TA muscle is implanted with a porous fibrillar collagen scaffold 15,20,42 after induction of VML, the implanted scaffold helps to retain the shape of the ablated muscle, in which the site of ablation becomes more evident (Fig. 4). Histological analyses can be used to visualize the partially degraded collagen scaffold at 3 weeks after implantation, where the collagen scaffold appears light pink in an H&E stain (Fig. 4a,b) or dark blue in the trichrome stain (Fig. 4c,d). The tissue sections may show signs of muscle regeneration as well as mild infiltration of inflammatory cells in the periphery of the scaffold. Acellular scaffolds may offer some therapeutic benefit but are not sufficient for the full restoration of muscle function and regeneration 15,20,25 .

Although the effect of VML injuries on other cell types is understudied, compared with healthy muscle, the ablated rat quadriceps muscle show notably fewer neuromuscular junctions as an indicator of innervation ¹². In the injured muscle, the majority of neuromuscular junctions were associated with fragmented morphology after 14 d. By day 28, the neuromuscular junctions showed either fragmented morphology or were forming new acetylcholine receptor clusters, but none showed normal innervation. Interestingly, the perfused vascular volume after 28 d was higher than in control uninjured model. These data suggest that VML injuries are also associated with nerve and vascular damage.

Reporting summary

Further information on research design is available in the Nature Portfolio Reporting Summary linked to this article.

Data availability

All data generated or analyzed during this study are derived from our original research study or are included in this paper. Source data are provided with this paper.

Received: 22 July 2022; Accepted: 24 May 2024;

Published online: 18 October 2024

References

- Grogan, B. F., Hsu, J. R. & Skeletal Trauma Research Consortium. Volumetric muscle loss. J. Am. Acad. Orthop. Surg. 19, S35–S37 (2011).
- Mauro, A. Satellite cell of skeletal muscle fibers. J. Biophys. Biochem. Cytol. 9, 493–495 (1961)
- Caldwell, C. J., Mattey, D. L. & Weller, R. O. Role of the basement membrane in the regeneration of skeletal muscle. Neuropathol. Appl. Neurobiol. 16, 225–238 (1990).
- Lefaucheur, J. P. & Sebille, A. The cellular events of injured muscle regeneration depend on the nature of the injury. Neuromuscul. Disord. 5, 501–509 (1995).
- Aguilar, C. A. et al. Multiscale analysis of a regenerative therapy for treatment of volumetric muscle loss injury. Cell Death Discov. 4, 1–11 (2018).
- Corona, B. T., Wenke, J. C. & Ward, C. L. Pathophysiology of volumetric muscle loss injury. Cells Tissues Organs 202, 180–188 (2016).
- Greising, S. M., Dearth, C. L. & Corona, B. T. Regenerative and rehabilitative medicine: a necessary synergy for functional recovery from volumetric muscle loss injury. Cells Tissues Organs 202, 237–249 (2016).
- Nakayama, K. H., Shayan, M. & Huang, N. F. Engineering biomimetic materials for skeletal muscle repair and regeneration. Adv. Healthc. Mater. 8, e1801168 (2019).
- Shayan, M. & Huang, N. F. Pre-clinical cell therapeutic approaches for repair of volumetric muscle loss. *Bioengineering* https://doi.org/10.3390/bioengineering7030097 (2020).
- Dziki, J. et al. An acellular biologic scaffold treatment for volumetric muscle loss: results of a 13-patient cohort study. NPJ Regen. Med. 1, 16008 (2016).
- Nakayama, K. H. et al. Treatment of volumetric muscle loss in mice using nanofibrillar scaffolds enhances vascular organization and integration. Commun. Biol. 2, 170 (2019).
- Anderson, S. E. et al. Determination of a critical size threshold for volumetric muscle loss in the mouse quadriceps. Tissue Eng. Part C. Methods 25, 59–70 (2019).
- Garg, K. et al. Volumetric muscle loss: persistent functional deficits beyond frank loss of tissue. J. Orthop. Res. 33, 40–46 (2015).
- Willett, N. J. et al. Attenuated human bone morphogenetic protein-2-mediated bone regeneration in a rat model of composite bone and muscle injury. Tissue Eng. C. 19, 316–325 (2013).
- Hu, C. et al. Comparative effects of basic fibroblast growth factor delivery or voluntary exercise on muscle regeneration after volumetric muscle loss. *Bioengineering* 9, 37 (2022).
- Larouche, J. A., Wallace, E. C., Spence, B. D., Buras, E. & Aguilar, C. A. Spatiotemporal mapping of immune and stem cell dysregulation after volumetric muscle loss. JCI Insight https://doi.org/10.1172/jci.insight.162835 (2023).
- Corona, B. T., Henderson, B. E., Ward, C. L. & Greising, S. M. Contribution of minced muscle graft progenitor cells to muscle fiber formation after volumetric muscle loss injury in wild-type and immune deficient mice. *Physiol. Rep.* 5, e13249 (2017).
- Pollot, B. E. & Corona, B. T. Volumetric muscle loss. Methods Mol. Biol. 1460, 19–31 (2016).
- Quarta, M. et al. Bioengineered constructs combined with exercise enhance stem cell-mediated treatment of volumetric muscle loss. Nat. Commun. 8, 15613 (2017).
- Nakayama, K. H. et al. Rehabilitative exercise and spatially patterned nanofibrillar scaffolds enhance vascularization and innervation following volumetric muscle loss. NPJ Regen. Med. 3. 16 (2018).
- Quarta, M. et al. Biomechanics show stem cell necessity for effective treatment of volumetric muscle loss using bioengineered constructs. NPJ Regen. Med. 3, 18 (2018).
- Corona, B. T. et al. Further development of a tissue engineered muscle repair construct in vitro for enhanced functional recovery following implantation in vivo in a murine model of volumetric muscle loss injury. Tissue Eng. Part A 18, 1213–1228 (2012).
- Sicari, B. M. et al. An acellular biologic scaffold promotes skeletal muscle formation in mice and humans with volumetric muscle loss. Sci. Transl. Med. 6, 234ra258 (2014).
- Zaitseva, T. S. et al. Aligned nanofibrillar scaffolds for controlled delivery of modified mRNA. Tissue Eng. Part A 25, 121–130 (2019).

- Alcazar, C. A., Hu, C., Rando, T. A., Huang, N. F. & Nakayama, K. H. Transplantation of insulin-like growth factor-1 laden scaffolds combined with exercise promotes neuroregeneration and angiogenesis in a preclinical muscle injury model. *Biomater. Sci.* 8, 5376–5389 (2020).
- Corona, B. T. et al. Autologous minced muscle grafts: a tissue engineering therapy for the volumetric loss of skeletal muscle. Am. J. Physiol. Cell Physiol. 305, C761–775 (2013).
- Sirabella, D., De Angelis, L. & Berghella, L. Sources for skeletal muscle repair: from satellite cells to reprogramming. J. Cachexia Sarcopenia Muscle 4, 125–136 (2013).
- Wu, X., Corona, B. T., Chen, X. & Walters, T. J. A standardized rat model of volumetric muscle loss injury for the development of tissue engineering therapies. *Biores. Open Access* 1, 280–290 (2012).
- Sicherer, S. T., Venkatarama, R. S. & Grasman, J. M. Recent trends in injury models to study skeletal muscle regeneration and repair. *Bioengineering* https://doi.org/10.3390/ bioengineering7030076 (2020).
- Owens, B. D. et al. Combat wounds in operation Iraqi Freedom and operation Enduring Freedom. J. Trauma 64, 295–299 (2008).
- Merritt, E. K. et al. Repair of traumatic skeletal muscle injury with bone-marrow-derived mesenchymal stem cells seeded on extracellular matrix. Tissue Eng. A 16, 2871–2881 (2010).
- Gamba, P. G. et al. Experimental abdominal wall defect repaired with acellular matrix. Pediatr. Surg. Int. 18, 327–331 (2002).
- VanDusen, K. W., Syverud, B. C., Williams, M. L., Lee, J. D. & Larkin, L. M. Engineered skeletal muscle units for repair of volumetric muscle loss in the tibialis anterior muscle of a rat. Tissue Eng. A 20, 2920–2930 (2014).
- Carleton, M. M., Locke, M. & Sefton, M. V. Methacrylic acid-based hydrogels enhance skeletal muscle regeneration after volumetric muscle loss in mice. *Biomaterials* 275, 120909 (2021).
- Dolan, C. P. et al. The impact of bilateral injuries on the pathophysiology and functional outcomes of volumetric muscle loss. NPJ Regen. Med. 7, 59 (2022).
- Corona, B. T., Rivera, J. C., Dalske, K. A., Wenke, J. C. & Greising, S. M. Pharmacological mitigation of fibrosis in a porcine model of volumetric muscle loss injury. *Tissue Eng. A* 26, 636–646 (2020).
- Greising, S. M. et al. Unwavering pathobiology of volumetric muscle loss injury. Sci. Rep. 7, 13179 (2017).
- Novakova, S. S. et al. Repairing volumetric muscle loss in the ovine peroneus tertius following a 3-month recovery. Tissue Eng. A 26, 837–851 (2020).
- Ibrahim, M. M. et al. Modifying hernia mesh design to improve device mechanical performance and promote tension-free repair. J. Biomech. 71, 43–51 (2018).
- Langford, D. J. et al. Coding of facial expressions of pain in the laboratory mouse. Nat. Methods 7, 447–449 (2010).
- Clark, A. et al. Myogenic tissue nanotransfection improves muscle torque recovery following volumetric muscle loss. NPJ Regen. Med. 7, 63 (2022).
- Nakayama, K. H. et al. Aligned-braided nanofibrillar scaffold with endothelial cells enhances arteriogenesis. ACS Nano 9, 6900–6908 (2015).

Acknowledgements

This research received funding from the Alliance for Regenerative Rehabilitation Research and Training (AR3T), which is supported by the Eunice Kennedy Shriver National Institute of Child Health and Human Development (NICHD), National Institute of Neurological Disorders and Stroke (NINDS) and National Institute of Biomedical Imaging and Bioengineering (NIBIB) of the National Institutes of Health under Award Number P2CHD086843. This study was supported by grants to N.F.H. from the US National Institutes of Health (R01 HL142718, R41HL170875 and R21 HL172096-01), the National Science Foundation (1829534 and 2227614) and the Department of Veterans Affairs (RX001222 and 1101BX004259). N.F.H is a recipient of a Research Career Scientist award (IK6BX006309) from the Department of Veterans Affairs. K.H.N. was supported by grants from the National Institutes of Health (R01AR080150, R00HL136701) and AR3T (CNVA00048860).

Author contributions

C.A., C.H., M.Q. and K.H.N. optimized the muscle ablation model and scaffold implantation procedure. G.C. and A.H.-P.C provided technical assistance with tissue histology. N.F.H. and T.A.R. interpreted the data. C.A., C.H. and N.F.H. planned and wrote the manuscript, with input from all authors. All authors gave approval for the final version to be published.

Competing interests

The authors declare no competing interests.

Additional information

 $\textbf{Supplementary information} \ The online version contains supplementary material available at \ https://doi.org/10.1038/s41596-024-01059-y.$

Correspondence and requests for materials should be addressed to Ngan F. Huang.

Peer review information *Nature Protocols* thanks Kimberley Huey, Pablo Fernandez-Marcos and the other, anonymous, reviewer(s) for their contribution to the peer review of this work.

Reprints and permissions information is available at www.nature.com/reprints.

Publisher's note Springer Nature remains neutral with regard to jurisdictional claims in published maps and institutional affiliations.

Related links

Key references using this protocol

Hu, C. et al. *Bioengineering* **9**, 37 (2022): https://doi.org/10.3390/bioengineering9010037 Alcazar, C. A. et al. *Biomat. Sci.* **8**, 5376–5389 (2020): https://doi.org/10.1039/d0bm00990c Quarta, M. et al. *NPJ Regen. Med.* **3**, 18 (2018): https://doi.org/10.1038/s41536-018-0057-0 Quarta, M. et al. *Nat. Commun.* **8**, 15613 (2017): https://doi.org/10.1038/ncomms15613

This is a U.S. Government work and not under copyright protection in the US; foreign copyright protection may apply 2024

nature research

Corresponding author(s):	Ngan Huang
Last updated by author(s):	05/06/2024

Reporting Summary

Nature Research wishes to improve the reproducibility of the work that we publish. This form provides structure for consistency and transparency in reporting. For further information on Nature Research policies, see our Editorial Policies and the Editorial Policy Checklist.

o.			
St	at	ıst	$1 \cap S$

For	all statistical analyses, confirm that the following items are present in the figure legend, table legend, main text, or Methods section.
n/a	Confirmed
	The exact sample size (n) for each experimental group/condition, given as a discrete number and unit of measurement
	A statement on whether measurements were taken from distinct samples or whether the same sample was measured repeatedly
	The statistical test(s) used AND whether they are one- or two-sided Only common tests should be described solely by name; describe more complex techniques in the Methods section.
\boxtimes	A description of all covariates tested
\boxtimes	A description of any assumptions or corrections, such as tests of normality and adjustment for multiple comparisons
	A full description of the statistical parameters including central tendency (e.g. means) or other basic estimates (e.g. regression coefficient) AND variation (e.g. standard deviation) or associated estimates of uncertainty (e.g. confidence intervals)
	For null hypothesis testing, the test statistic (e.g. <i>F</i> , <i>t</i> , <i>r</i>) with confidence intervals, effect sizes, degrees of freedom and <i>P</i> value noted <i>Give P values as exact values whenever suitable.</i>
\boxtimes	For Bayesian analysis, information on the choice of priors and Markov chain Monte Carlo settings
\boxtimes	For hierarchical and complex designs, identification of the appropriate level for tests and full reporting of outcomes
\boxtimes	Estimates of effect sizes (e.g. Cohen's <i>d</i> , Pearson's <i>r</i>), indicating how they were calculated
	Our web collection on <u>statistics for biologists</u> contains articles on many of the points above.

Software and code

Policy information about availability of computer code

Data collection Data

Data is collected in the form of intraoperative images and histological images; measurements of muscle weights and sizes. No softwares were used for data collection

Data analysis

Means and standard deviation calculations were made using Microsoft Excel. Student's t-test or analysis of variance was performed using Graphpad Prism software (v.9)

For manuscripts utilizing custom algorithms or software that are central to the research but not yet described in published literature, software must be made available to editors and reviewers. We strongly encourage code deposition in a community repository (e.g. GitHub). See the Nature Research guidelines for submitting code & software for further information.

Data

Policy information about availability of data

All manuscripts must include a data availability statement. This statement should provide the following information, where applicable:

- Accession codes, unique identifiers, or web links for publicly available datasets
- A list of figures that have associated raw data
- A description of any restrictions on data availability

All data generated or analyzed during this study are derived from our original research study or are included in this paper. Source data for quantitative data are provided in the data supplement with this paper.

Field-specific reporting			
Please select the or	ne below t	hat is the best fit for your research. If you are not sure, read the appropriate sections before making your selection.	
∠ Life sciences	[Behavioural & social sciences	
For a reference copy of t	the documen	t with all sections, see <u>nature.com/documents/nr-reporting-summary-flat.pdf</u>	
Life scier	nces	study design	
All studies must dis	sclose on t	hese points even when the disclosure is negative.	
Sample size	Table 1: n Fig 3a: n=	=5 2-mm punch group; n=6 3-mm punch group 5	
Data exclusions	No data w	vas excluded	
Replication	The repro	ducibility of the surgical procedures have been validated by our cited publications	
Randomization		strate the principles of the surgical procedure, randomization was not needed. For the data in Table 1 and Fig 3a, the animals were mly assigning to treatment groups.	
Blinding	Blinding was not necessary, as the difference in ablation size between the 2- and 3-mm punch groups is visually obvious and cannot be blinded at the time of data acquisition.		
Reporting for specific materials, systems and methods We require information from authors about some types of materials, experimental systems and methods used in many studies. Here, indicate whether each material, system or method listed is relevant to your study. If you are not sure if a list item applies to your research, read the appropriate section before selecting a response. Materials & experimental systems Methods			
Antibodies used		aminin	
Validation	7	The laminin antibody has been validated to stain the muscle fiber periphery (Fig. 4).	
Animals and other organisms			
Policy information about <u>studies involving animals</u> ; <u>ARRIVE guidelines</u> recommended for reporting animal research			
Laboratory anima	Laboratory animals C56/BL6 male mice, 7-18 weeks old		

Laboratory animals

C56/BL6 male mice, 7-18 weeks old

Wild animals

none

Field-collected samples

none

All animal studies were approved by the Institutional Animal Care and Use Committee at the Veterans Affairs Palo Alto Health Care System

Note that full information on the approval of the study protocol must also be provided in the manuscript.